Current Chemistry Letters 13 (2024) 265–276

Contents lists available at GrowingScience

Current Chemistry Letters

homepage: www.GrowingScience.com

Photocatalytic degradation of Orange-II by surfactant assisted Mn/Mg co-doped TiO_2 nanoparticles under visible light irradiation

Sankara Rao Miditana[a], Siva Rao Tirukkovalluri[b*], Imandi Manga Raju[b] and Shaik Abdul Alim[b]

[a]*Department of Chemistry, Govt. Degree College, Puttur, Tirupati, Andhra Pradesh, India-517583*
[b]*Department of Inorganic & Analytical Chemistry, A.U. College of Science & Technology, Andhra University, Visakhapatnam, Andhra Pradesh, India-530003*

C H R O N I C L E

Article history:
Received December 25, 2022
Received in revised form
June 2, 2023
Accepted June 14, 2023
Available online
June 14, 2023

Keywords:
Mn/Mg nanoparticles
Anionic Surfactant
AO7-Degradation
Visible light
Photoluminescence

A B S T R A C T

In this research, the photocatalytic effect was studied for sol-gel synthesized Mn/Mg co-doped metal oxide (TiO_2) nanoparticles (NPs), which are encapsulated with anionic Gemini surfactant. The physicochemical properties of Mn/Mg co-doped TiO_2 were investigated using a variety of characterization techniques, FT-IR, UV Vis-DRS, XRD, SEM, EDX, TEM, BET and PL. Characterization results reveal that Mn/Mg dopants stabilize TiO_2 in the form of anatase phase and reduce the bandgap energy. Presence of strong chemical bonding and functional groups at the interface of dopant and TiO_2 NPs was confirmed with FT-IR. The photocatalytic activity of these catalysts was assessed by the degradation of Orange II (AO7) using visible light irradiation. Of the variable nanomaterials MMT5-GS2 showed remarkable results. The photoluminescence studies revealed that OH radicals are the reactive species and responsible for oxidative photocatalytic degradation of Orange II.

1. Introduction

During recent years numerous hazardous persistent organic contaminants have been discharging into the environment due to widespread intensive industrial activities which are capable of penetration deep into the soil and reaching groundwater due to their chemical stability, sufficient water solubility and resistance to biodegradation. Hence, it is essential to remove these chemically stable and persistent organic pollutants from contaminated water. But ensuring the safety of applied materials in these applications is crucial to minimize any potential adverse effects on ecosystems, human health, and the overall sustainability of the environment. Hence, we have selected the TiO_2 nanoparticles due to its extraordinary photocatalytic activity, non-toxicity, high availability, biocompatibility, and low price.[1] TiO_2 has been utilized for many years as an inert, non-toxic pigment product or other substance evaluated by many regulatory bodies such as the Material Safety Data Sheets (MSDS) and others charged with the responsibility of safeguarding the health of occupational workers and public health safety.[2]

TiO_2 is the advantageous among the variable semiconductors that are being studied from the past few decades for the photocatalytic degradation of various organic pollutants from wastewater due to its band gap, electronic structure, chemical inertness and commercial availability. To make it suitable for visible light activity, many attempts have been made to alter the electronic structure of TiO_2 to conquer the disadvantages of large bandgap energy and high electron-hole recombination rate. The recent literature findings reported that transition metal ion doping into TiO_2 crystal lattice had overcome the above drawbacks and appreciably enhanced its visible light activity.[3-5] The interaction of transition metal ion dopant's 3d or 4d states with the Ti 3d states results in an additional energy level below the conduction band of TiO_2, which significantly

* Corresponding author. Tel.: +91 7702110459
E-mail address sivaraoau@gmail.com (S. R. Tirukkovalluri)

doi: 10.5267/j.ccl.2023.6.003

lowers the band gap energy and electron-hole recombination compared to other metal ion dopants currently under study.[6] Recently, Lakshmi et al. reported that Manganese is most preferable among the transition metals owing to the presence of t_2g orbital of d is much close to conduction band of TiO_2 by which the absorption can be possibly shifted to visible part of the spectrum.[7] On the other hand, Zhang et al., Meshesha et al., and Sofianou et al. investigated the effect of Magnesium, an alkaline earth metal on the crystalline structure and catalytic activity of TiO_2 and found its absorption band was shifted more towards visible region, which led to strong photocatalytic performance.[8-10] Hence, Mn^{2+} and Mg^{2+} ions could be more effective as metal ion dopants to modify the TiO_2 for better photocatalytic performance under visible light irradiation.

Since the size, shape, and surface area of photocatalysts play important roles in the photocatalytic degradation of organic pollutants in wastewater, surfactants have been the best reported species for controlling nanoparticle growth and agglomeration during the synthesis. Among the various surfactants, 1,4-butanesultone, a Gemini surfactant with stronger surface activity, is the most suitable as an end-capping agent to prepare spherical bimetallic TiO_2 NPs with small particle size and large surface area.[11] Therefore, in this study, we aimed to synthesize Mn^{2+} and Mg^{2+} bimetallic TiO_2 NPs using a sol-gel process in the presence of Gemini surfactant, by which we can synthesize TiO_2 NPs under stoichiometric control with high purity and homogeneous materials at room temperature.[12]

Compared with bulk materials, nanomaterials have unique physical, chemical and mechanical properties. To understand the overall properties, it is important to characterize the structural, optical and morphological properties of nanomaterials for better results before using them in different applications.[13] Therefore, in this study, several advanced and sophisticated techniques were employed to characterize the crystal phase, surface morphology, elemental composition, visible light absorption capacity, particle size and surface area of the synthesized bimetallic doped titania NPs to understand their applicability for photocatalytic degradation applications.

Due to the huge industrial activities, various organic dye pollutants are being discharged into water bodies causing water pollution. During synthesis and processing around 17% of the dyes produced worldwide affect the water resources. Moreover, 49% dyes used in industries are poisonous azo dyes, which are characterized by one or more azo bonds[14] among which, Orange II (AO7) is a familiar azo dye, which is used in the paper printing, textile dyeing, and leather industries extensively.[15] It is a probable carcinogen that affects the skin, eyes, respiratory system, and digestive tract.[16]

Hence, our research concern is removal of pollutants from contaminated water in a green way. Therefore, by using synthesized Mn and Mg co-doped TiO_2 nano catalyst, we attempted to remove this model azo dye pollutant from the contaminated water. The photocatalytic activity of supreme nano catalyst was examined by optimizing the important reaction parameters like dopant concentration, surfactant concentration, solution pH, catalyst dosage and initial concentration of the dye for the better effect of the pollutant.

2. Experimental

2.1 Materials

Without additional purification, reagent-grade compounds of all types were employed in this study. Titanium tetra-n-butoxide ($Ti(OBu)_4$), Manganese nitrate $[Mn(NO_3)_2]6H_2O$ and Magnesium Nitrate $[Mg(NO_3)_2]6H_2O$ purchased from E-Merck Germany were used as precursors of TiO_2, Mn and Mg respectively, for preparing Mn^{2+}/Mg^{2+} doped TiO_2 samples. 1,4-Butane sultone from Sigma Aldrich (Germany) was used for the surfactant assisted metal doped TiO_2 catalysts. As a model azo dye pollutant for studies on photocatalytic degradation, Orange II (High media, India) was utilized. Milli-Q water used for the preparation of all the solutions.

2.2 Synthesis of Photocatalyst

Gemini surfactant-supported Mn^{2+}/Mg^{2+} doped TiO_2 samples were prepared using sol-gel technique. During this procedure, titanium tetra-n-butoxide (10 mL) was added to ethanol (20 mL), acidified with 1.4 mL HNO_3, placed in a Pyrex glass jar (Solution-I) and stirred for 20 min. Desired wt% (0.25 wt% - 1.0 wt%) of Mn^{2+} and Mg^{2+} dopants proportional to the weight of TiO_2 into ethanol (20 mL) were taken in another beaker and added 4.5 mL of Milli-Q water to achieve efficient hydrolysis (Solution-II). Then, Solution-II was slowly added dropwise to Solution-I with continuous stirring. The colloidal solution formed after complete mixing was stirred for another 90 min and aged for 48 h to obtain a gel. The formed gel was dried (at 70 ^oC), ground and calcined in an oven at 450 ^oC for about 5 h. After the sample has cooled, and ground sufficiently to obtain a homogeneous powder. In order to optimize the optimal doping concentration, the photocatalytic efficiency of the synthesized bimetallic doped TiO_2 samples was tested by degrading Orange II dye, and it was found that 0.25 wt% Mn^{2+} and 1.00 wt% Mg^{2+} doped TiO_2 (MMT5) were the best. To further enhance the photocatalytic activity of MMT5 catalysts, gemini surfactant-supported MMT5 nanocatalysts were synthesized following the same procedure, including the addition of gemini surfactant (5 wt %, 10 wt% and 15 wt %)-after mixing solution-I and solution-II. To investigate and compare the effects of dopants and surfactants on the photocatalytic performance of metallic doped titania, undoped titania samples were prepared using the same procedure without the addition of dopants and surfactant precursors. Details of all synthesized catalysts are shown in **Table 1**.

Table. 1. Names assigned to prepared TiO_2 NPs

S.No.	Weight percentages of dopants (Wt %)		Gemini Surfactant (Wt %)	Name given to the Sample
1	0.25 Mn^{2+}	1.00 Mg^{2+}	-	MMT5
2	0.25 Mn^{2+}	1.00 Mg^{2+}	5	MMT5-GS1
3	0.25 Mn^{2+}	1.00 Mg^{2+}	10	MMT5-GS2
4	0.25 Mn^{2+}	1.00 Mg^{2+}	15	MMT5-GS3
5	NIL		-	Undoped-TiO_2

2.3 Experimental procedure for determination of visible light photocatalytic activity of nanocatalyst

The photocatalytic activity of surfactant-supported TiO_2 nanocatalysts doped with Mn^{2+}/Mg^{2+} bimetal ions was investigated by degrading the model azo dye pollutant Orange II in a previously described visible light photoreactor.[17]. For visible light illumination, a high-pressure metal halide lamp (400 W, 35,000 lm, 436-546 nm output) placed at a distance of 20 cm from the reaction vessel containing 100 mL of AO7 dye solution of the desired concentration (1-10 mgL^{-1}) and catalyst. To shield the IR effect and keep the temperature (25 °C) constant during the degradation experiments, water was continuously passed around the reaction vessel. Before visible light irradiation, pH of the reaction mixture was adjusted to the desired value by adding 0.1 N NaOH/0.1 N HCl, and stirred the reaction mixture in the dark for 30 min to reach adsorption-desorption equilibrium between AO7-dye and catalyst's surfaces.[18] After the visible light irradiation, 5 mL aliquots of samples were collected at regular time intervals using Millipore syringe (0.45 µm) and change in the concentration of AO7 dye was measured by its absorbance at 525 nm, on a UV-vis spectrophotometer (Shimadzu 1601). The percentage degradation of AO7 was determined by using the following equation.[19]

$$\% \text{ degradation of AO7} = \quad 1\text{-}C/C_0 \times 100$$

where C_0 is the initial concentration of the AO7 dye solution before degradation and C is the concentration at time t. For better photocatalytic degradation, the effects of reaction parameters such as dopant concentration, surfactant concentration, solution pH, catalyst dosage, and initial dye concentration were studied and optimized by changing the measurement parameters while keeping other parameters unchanged. The results are discussed in Sections 4.1-4.5. Since the photocatalytic degradation of organic pollutants is mainly initiated by strongly oxidizing OH radicals, which are easily captured by fluorescent probes, photoluminescence (PL) technology was used to study the photocatalytic process with coumarin as a probe molecule.[19]

3. Results and Discussion

3.1 X-ray Diffraction Study

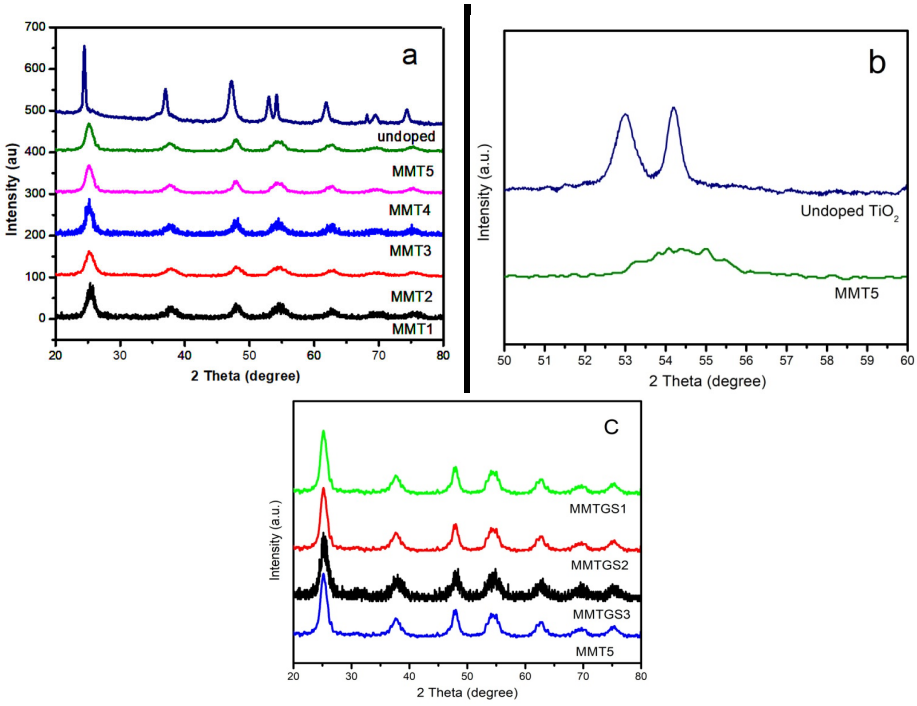

Fig. 1. (a) XRD patterns of undoped TiO_2 and Mn^{2+}/Mg^{2+} doped TiO_2 catalysts, **(b)** Zoom image of undoped TiO_2 and MMT5 and **(c)** MMT5 and Surfactant assisted (MMT5-GS1- MMT5-GS3).

All prepared samples (**Fig. 1a-c**) including undoped TiO_2 produced anatase peaks at 2θ values of 25.3º, 37.9º, 48.05º and 54.1º corresponding to (101), (004), (200) and (211) planes of anatase phase (JCPDS No. 21-1272). No additional peak was found at 2θ = 27.8°, indicating no rutile phase formation. Since the ionic radii of Mn^{2+} (0.78 Å) and Mg^{2+} (0.72 Å) are closer to those of Ti^{4+} (0.68 Å), it is expected that the Mn^{2+} and Mg^{2+} doped metal ions will replace the Ti^{4+} ions in the TiO_2 matrix. This is confirmed by the absence of any diffraction peaks associated with Mg oxides or other compounds.[20,21] And it is well known that since Mn^{2+} and Mg^{2+} are more electropositive, the electron cloud can remain loose in any TiO_2, favoring the formation of a less dense anatase phase.[22] The average crystallite size of undoped TiO_2, MMT and MMT-GS catalysts was calculated based on the full width at half maximum (FWHM) of the characteristic high intensity peak using the Scherrer equation, $d = k\lambda/\beta \cos\theta$, where d is the average crystallite size, k is 0.9 (Scherrer's constant), λ is 1.5406 Å (X-ray wavelength), β is the FWHM and θ is the diffraction angle, listed in Table 2. As can be seen from the table, the average crystallite size of the catalysts ranges from 7.21-10.22 nm, 10.86-12.87 nm and 18.30 nm for MMT-GS, MMT and undoped TiO_2 nanocatalysts. Substitutional doping of metal ions into the TiO_2 lattice suppresses grain growth by forming Ti-O-Mn and Ti-O-Mg, thereby reducing the crystallite size in MMT catalysts. Additional reduction in crystallite size was seen for the surfactant-prepared catalyst, which can be attributed to the Gemini surfactant's efficient coping abilities which controls the nucleation and minimizes the agglomeration of TiO_2 NPs during synthesis process.[23]

3.2 UV-Visible Diffuse Reflectance Spectra Study (UV–vis. DRS)

UV-vis. diffuse reflectance spectra of undoped TiO_2, MMT and MMT-GS nanomaterials shown in **Fig. 2a**. It can be seen that the absorption bands of MMT and MMT-GS are shifted more strongly towards higher wavelengths (red shift) compared with undoped TiO_2, which may be due to the reduced bandgap by co-doping of Mn^{2+} and Mg^{2+} into the TiO_2 matrix. The narrowing of the band gap can be attributed to the combined action of these two metal dopant ions (Mn^{2+} and Mg^{2+}) in the MMT and MMT-GS systems, which form additional energy levels below the TiO_2 conduction band, thus electron-hole recombine by trapping electrons and enhance the absorption of visible light. This can be further confirmed by the bandgap energies obtained for all synthesized catalysts using the Kubelka-Monk form and the Tauc diagram method.[24] The corresponding band gap energy values are shown in **Table 2**. As can be seen from the table, the average bandgap values of the MMT-GS, MMT and undoped TiO_2 photocatalysts are in the range of 2.66-2.83 eV, 2.68-2.97 eV and 3.20 eV respectively. According to these findings, all MMT and MMT-GS catalysts are visible light active. Catalysts MMT5, MMT5-GS1, MMT5-GS2 and MMT5-GS3 have the same weight percentages of Mn and Mg; therefore, they have absorption peaks at almost the same wavelength. But in particular, MMT5-GS2 shows the lowest bandgap energy, i.e. 2.66 eV, among all MMT and GS-assisted bimetallic doped catalysts.

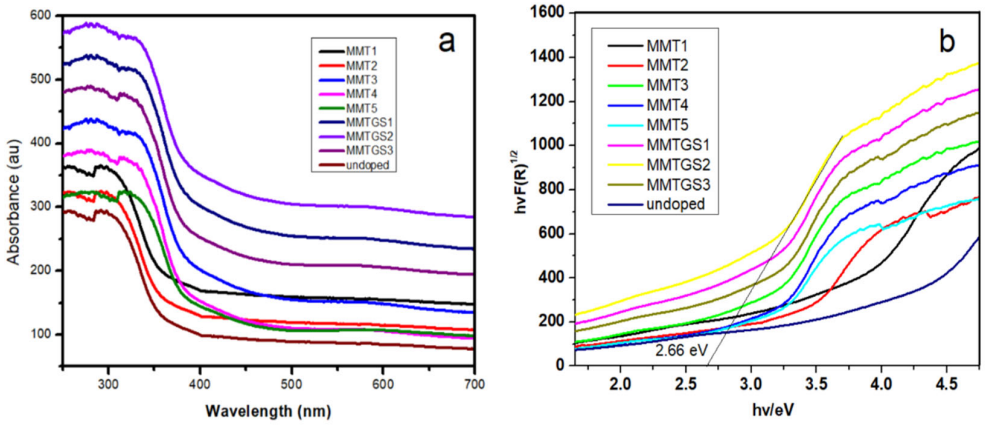

Fig. 2. (a) UV-Vis DRS and **(b)** Kubelka-Munk formalism spectra of undoped TiO_2, MMT and MMT5-GS catalysts.

Table. 2. The Results of crystallite size (XRD), Band gap (UV-VIS- DRS) and BET surface analysis.

S.No	Nanomaterials	Crystallite size (nm)	Band gap energy (eV)	BET surface analysis		
				Surface area (m^2/g)	Pore volume (cm^3/g)	Pore size (nm)
1	Undoped TiO_2	18.30	3.20	64.09	0.22	10
2	MMT5	10.86	2.68	112.03	0.24	7.0
3	MMT5-GS1	10.22	2.76	140.61	0.24	7.3
4	MMT5-GS2	7.21	2.66	230.20	0.25	6.4
5	MMT5-GS3	8.33	2.83	160.14	0.22	8.3

Before proceeding to the further characterization we have conducted trial photocatalytic degradation experiments for all the synthesized catalysts using AO7 dye. From the results it was noticed that among all the bimetal doped TiO_2 catalysts, 0.25 wt% Mn^{2+}& 1.00 wt% Mg^{2+} bimetal doped TiO_2 (MMT5) exhibited better photocatalytic activity. Furthermore, MMT5 supported with 10% GS (MMT-GS2) has exhibited greater photocatalytic activity. So, we chose these two specific catalysts for additional evaluation using SEM-EDX, TEM, BET, FT-IR, and photoluminescence analysis.

3.3 SEM- Energy Dispersive X- ray Spectroscopy

The FESEM images shown in **Fig. 3a**, **b** and **c** illustrate the surface morphology of undoped TiO_2, MMT5 and MMT5-GS2, respectively. On comparison, it can be clearly seen that the morphology of the TiO_2 has been changed from large aggregates with scratchy surface in undoped TiO_2 (**Fig. 3a**) to multiparticle agglomerated irregular shaped particles with rough surface in MMT5 and pseudospherical less agglomerated NPs with smooth surface area and less particle size in MMT-GS2. This is clearly indicating that Mg^{2+} and Mn^{2+} bimetal ions doping and capping action with Gemini surfactant have a significant impact on the morphology of TiO_2 NPs which controlled the grain growth and particle nucleation.

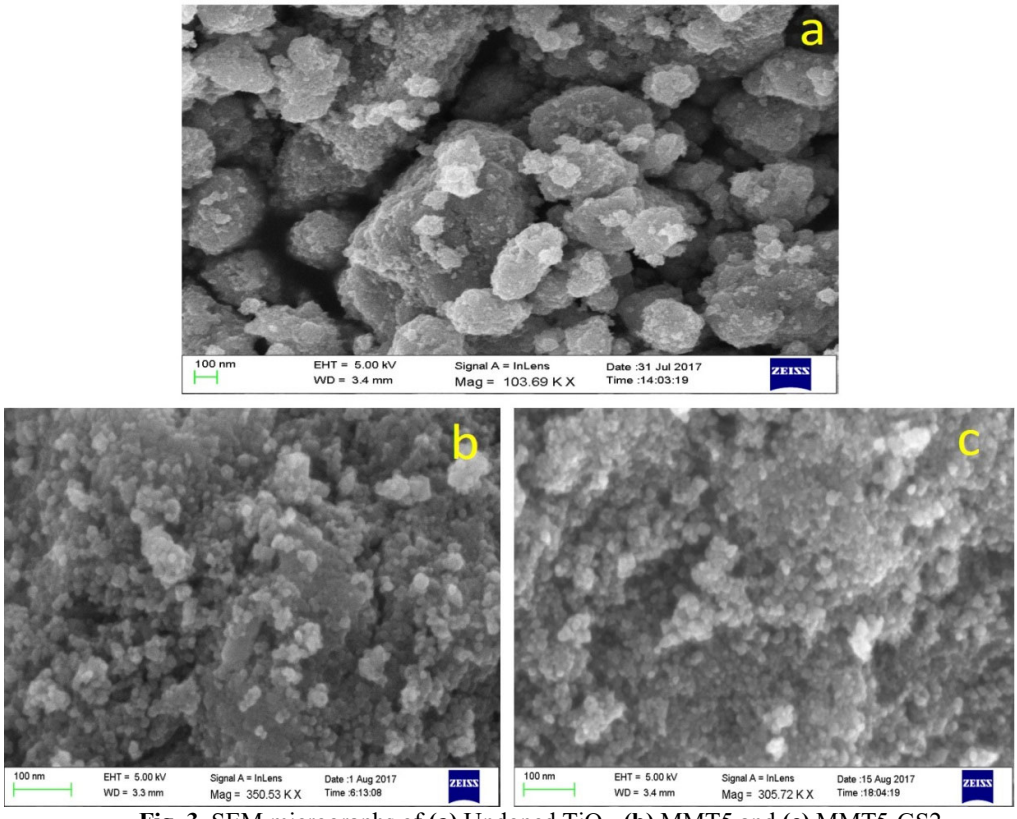

Fig. 3. SEM micrographs of **(a)** Undoped TiO_2, **(b)** MMT5 and **(c)** MMT5-GS2.

The MMT-GS2 samples were examined by EDX and the results are shown in **Fig. 4a**. The chemical composition is shown in **Fig. 4b**. Together with the Ti and O elements of TiO_2, doping elements Mn and Mg were found in the spectrum, supporting the presence of dopants in the TiO_2 matrix, and no peaks associated with GS were found in the spectrum, indicating complete elimination of GS after calcination.

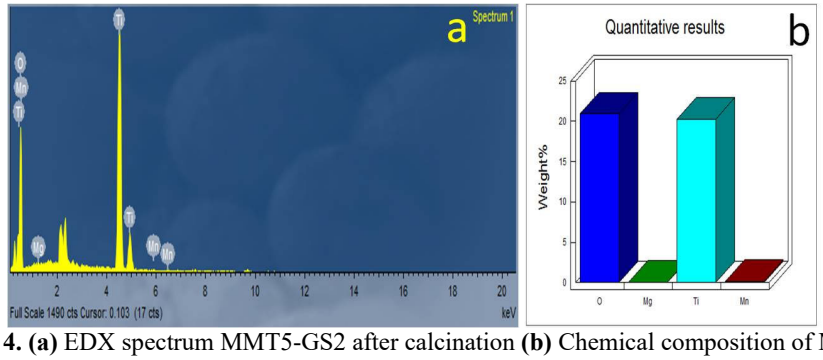

Fig. 4. (a) EDX spectrum MMT5-GS2 after calcination **(b)** Chemical composition of MMT5

3.4 Transmission Electron Microscope (TEM)

In Fig. **5a** and **5b** the TEM images of the MMT5 and MMT5-GS2 photocatalysts are given respectively. The bimetal doped TiO_2 (MMT-5) TEM image (**Fig. 5a**) displays pseudospherical shapes with multiparticle agglomeration and an average particle size of 6.6 nm. As objected to **Fig. 5a**, where the majority of the TiO_2 particles in MMT5-GS2 are well dispersed and exhibit very little agglomeration and the particle size is in the range of 2.3-5.4 nm, with an average particle size of 3.8 nm. Thus, it clearly indicates that the Gemini surfactant effectively inhibited the particle overgrowth and aggregation and resulted in less particle size with increased surface area, which is well correlated with BET results given in **Table 2**. The selected area electron diffraction (SAED) patterns shown in **Fig. 5c** confirmed the anatase phase with good crystallinity indexed by the concentric rings, which is in good agreement with XRD diffraction patterns. In addition to SAED, from the HR-TEM image of MMT5-GS2 (**Fig. 5d)** the observed lattice fringes with d-spacing of 0.352 nm correspond to (101) plane of anatase and further confirms the single crystal nature and high crystallinity of anatase TiO_2. [25]

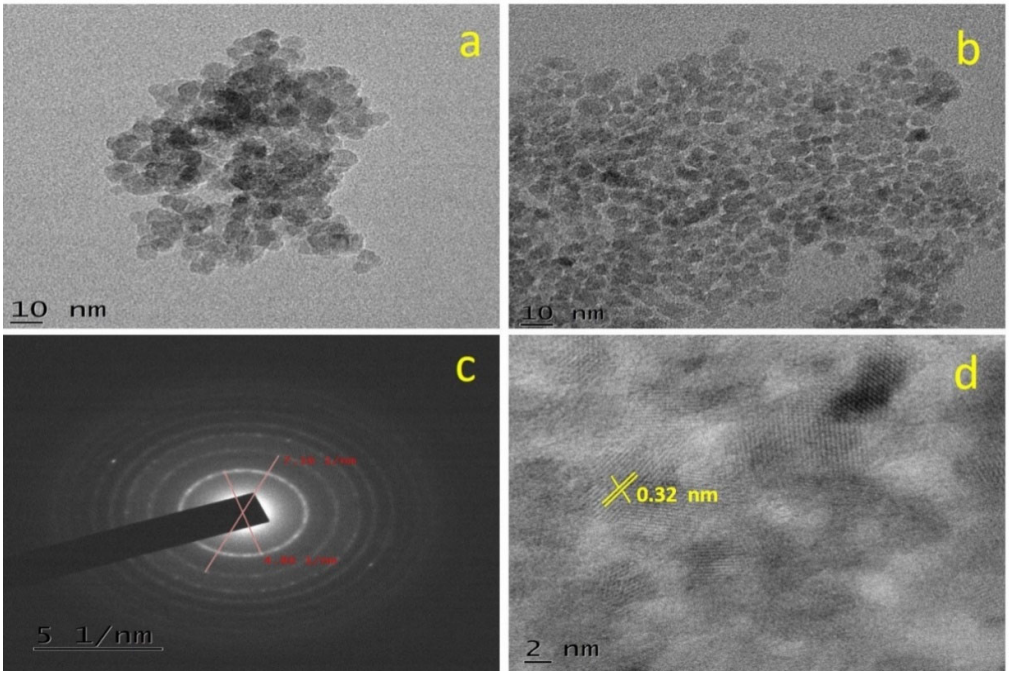

Fig. 5. TEM images of (**a**) MMT5, (**b**) MMT5-GS2, (**c**) SAED pattern and (**d**) MMT5-GS2 using HRTEM.

3.5 Fourier Transform Infrared Spectroscopy (FT-IR)

The incorporation of metal ion dopants, Mn^{2+} and Mg^{2+} into TiO_2 lattice was further confirmed by FT-IR results. Fig. 6a-d displays the FT-IR spectra of the MMT5, MMT5-GS2 (both before and after calcination) and the undoped TiO_2. The peaks at 3403.01 cm^{-1}, 2926.10 cm^{-1}, 1616.36 cm^{-1}, 1383.78 cm^{-1}, 3378.14 cm^{-1}, 2918.69 cm^{-1}, 1626.67 cm^{-1} and 1372.07 cm^{-1} are corresponding to stretching vibrations of surface O-H and 3351.79 cm^{-1}, 2918.72 cm^{-1}, 1619.40 cm^{-1} and 1383.80 cm^{-1} corresponds to the and bending vibrations of adsorbed H_2O molecules.[26] The stretching vibrations of Ti-O and bending vibrations of Ti-O-Ti observed at 575.41 cm^{-1} and 1375.78 cm^{-1} in undoped TiO_2 (**Fig. 6a**) were deformed/shifted to 620.32 cm^{-1} and 1300.12 cm^{-1} in MMT5 (**Fig. 6b**) and 540.01 cm^{-1} and 1182.01 cm^{-1} in MMT5-GS2 (**Fig. 6c & 6d**) respectively, which can be attributed to the presence of dopants in TiO_2 lattice. Hence, FT-IR study confirms that Mn^{2+} and Mg^{2+} are substitutionally doped into TiO_2 lattice by replacing Ti^{4+} and formed new network i.e Ti-O-Mn and Ti-O-Mg which are in good agreement with the previous reports.[27,28] The bands situated at about 2945.62 cm^{-1}, 1447.80 cm^{-1}, 1345.72 cm^{-1}, 1246.03 cm^{-1}, 1149.79 cm^{-1}, 1059.62 cm^{-1} and 996.59 cm^{-1} in GS were shifted to 2855.77 cm^{-1}, 1734.95 cm^{-1}, 1459.87 cm^{-1}, 1206.73 cm^{-1}, 1136.50 cm^{-1}, 1094.06 cm^{-1} and 982.86 cm^{-1} in MMT5-GS2 before calcinations (BC) shown in **Fig. 6c** which confirms the existence of strong electrostatic interaction between GS and catalyst surface of MMT5-GS2 before calcinations.[29]

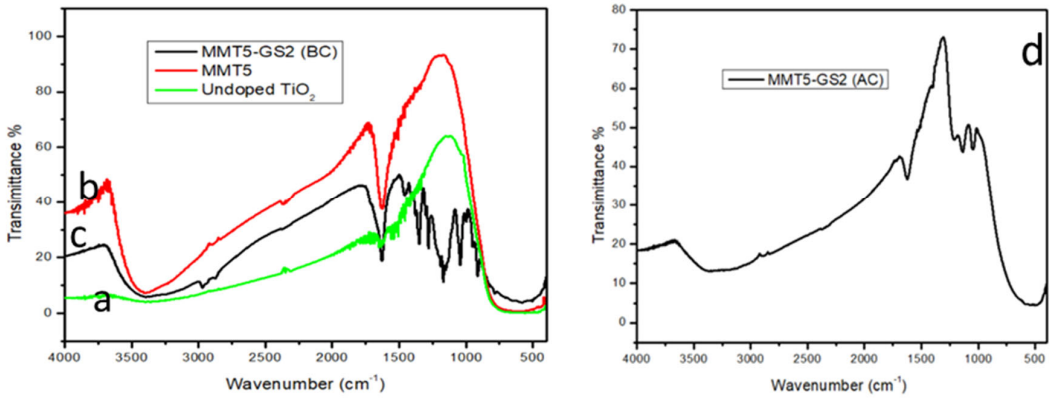

Fig. 6. (a) FT-IR spectra of undoped TiO_2, **(b)** MMT5 and **(c)** MMT5-GS2 (Before Calcination) and (**d)** FT-IR spectra of MMT5-GS2 (After Calcination).

From Fig. 6d, absence of these peaks confirms that there was no surfactant remained in the synthesized catalyst, MMT5-GS2 after calcinations (AC). This indicated that due to calcination at 450 °C, surfactant is completely eliminated from nanocatalyst.

3.6 Brunauer-Emmett-Teller (BET) surface area analysis

To examine the effect of bimetal doping and GS on the surface area and nature of the porosity of the as-produced TiO_2 nanoparticles of undoped TiO_2, MMT5 and MMT5-GS2N2, N2 adsorption-desorption isotherms and their corresponding Berret- Johner- Halenda (BJH) pore size distribution plots were recorded and presented in **Fig. 7a-b**. From **Fig. 7a**, it results in a type -IV isotherm with H2 hysteresis loop, characteristic of the ordered mesoporous structure of the catalyst.[30] The average surface area, ABET (m^2/g) of all prepared catalysts was determined and tabulated in **Table 2**.

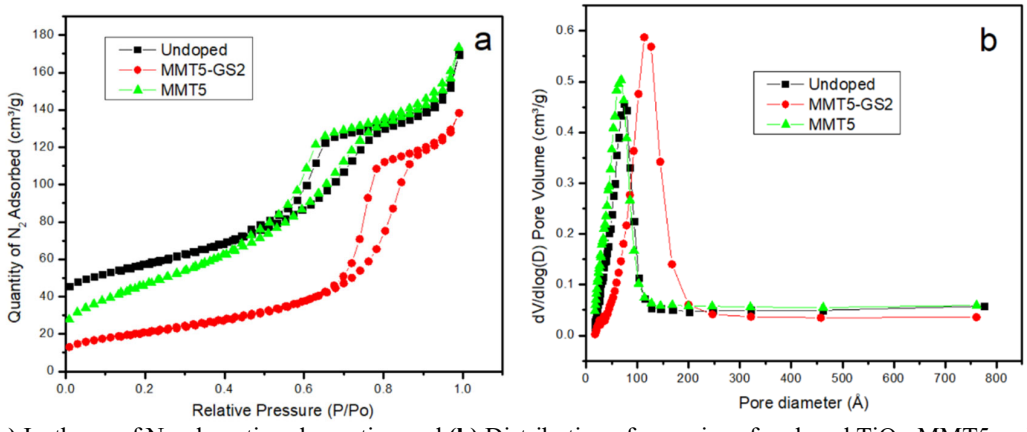

Fig. 7. (a) Isotherm of N_2 adsorption-desorption and **(b)** Distribution of pore size of undoped TiO_2, MMT5 and MMT5-GS2.

According to Table 2, the MMT has a larger surface area (112.03 m^2/g) than undoped TiO_2 (64.09 m^2/g) as a result of the dopants' suppression of crystal growth. In contrast, a catalyst made with GS surfactant (MMT5-GS2) has a greater surface area (230.20 m^2/g) than MMT5 and undoped TiO_2. It could be the strong evidence for the decreased particle size of the TiO_2 resulting from effective capping ability of the surfactant, which restricts the particle growth and nucleation during the synthesis process.

3.7 Photoluminescence Spectra (PL)

One of the essential reactive species in the process of photocatalysis is hydroxyl radical (•OH) and is responsible for oxidation reactions. Because of high reactivity and short life of hydroxyl radical, it is impossible for direct detection. To inspect the production of hydroxyl radicals from the catalyst during the photocatalysis reaction, photoluminescence technique has been adopted using coumarin as a fluorescent probe molecule, which on reaction with hydroxyl radicals yields the 7-hydroxy coumarin.[19] This method involves dispersing 0.10 g of catalyst in 100 mL of a 10 mg/L coumarin solution under acidic conditions, followed by illumination with visible light. Small aliquots of reaction solution samples were withdrawn for every 30 min, filtered and photoluminescence intensity was measured in the range of 350-600 nm with

excitation fixed at a wavelength of 435 nm. It has been observed from **Fig. 8** that in between 440-460 nm there exist photoluminescence spectra of the generated 7-hydroxycoumarin with maximum emission at 450 nm. A linear increase in photoluminescence intensity was observed with increasing irradiation time. However there was no activation of the sample in the absence of irradiation (0 min in **Fig. 8**).

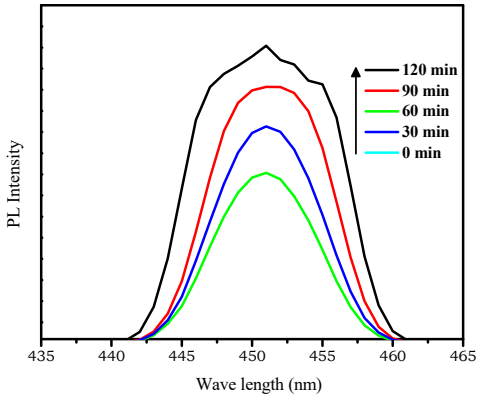

Fig. 8. PL spectra of MMT5-GS2.

From the above results, it could be understood that the number of hydroxyl radicals produced on the catalyst surface was directly proportional to the irradiation time. The outcomes further confirm that the produced nanomaterial had an accelerated rate of hydroxyl radical production when exposed to visible light. This is because the photo holes in the bimetal doped TiO_2 valence band, which had already formed, could instantly react with water to form a hydroxyl radical.[29]

4. Evaluation of photocatalytic activity of prepared nanocatalysts by degradation of Orange II (AO7)

The visible light-assisted catalytic activity of the synthesized MMT-GS photocatalyst was evaluated by degrading AO7. For better photocatalytic degradation, the effects of reaction parameters such as dopant concentration, surfactant concentration, solution pH, catalyst dosage, and initial dye concentration were investigated and optimized as follows.

4.1 Effect of Dopant (Mn & Mg) Concentration

To determine the optimal doping concentration of co-doped photocatalysts of the prepared TiO_2 nano catalysts, degradation experiments were carried out with photocatalysts and AO7 under visible light irradiation. The degradation rate of AO7 was detected by measuring the absorption of AO7, and the results are shown in **Fig. 9a**. As can be seen from the figure, when comparing with undoped TiO_2 all the bimetal doped TiO_2 photocatalysts have better photocatalytic performance under visible light irradiation. Among the synthesized photocatalysts, MMT5 exhibited the best catalytic performance, which can be attributed to the narrower bandgap, smaller crystallite size, and high surface area of co-doped TiO_2. Therefore, the presence of the two metal dopants increases the number of impurity levels between the valence and conduction bands, which helps to generate more electron-hole pairs.

4.2 Effect of Gemini surfactant concentration

Out of all the above, MMT5 catalyst has shown the ability of high photocatalytic activity because the number of trapped charge carriers increases per particle. Therefore, it was noticed that further applications are to be done on the basis of MMT5 catalyst with compilation of various weight percentages of Gemini surfactant (5 wt%, 10 wt% and 15 wt%) and maintain other conditions constant. To know the optimum concentrations of the GS in MMT5 of co-doped nanotitania on the photocatalytic degradation of AO7, experiments were carried out under visible light irradiation. The C/C_O degradation and rate reaction of AO7 has been quantified by measuring the absorbance of AO7 concentration and the results are presented in **Fig. 9b**. MMT5 with 10 wt% gemini surfactant has shown best activity.

4.3 Effect of pH of Solution

The solution pH is an important parameter for the catalytic efficiency of the MMT5-GS2 catalyst, as the solution pH changes the charges on the surface of the catalyst and dye molecules. The catalytic process was followed by a catalyst dose of 0.1 g and an initial dye concentration of 10 mg/L kept constant, the pH was varied between 2 to 8, and the reaction mixture was kept at 25 °C. **Fig. 9c** represents the degradation of MMT5-GS2 at different pH values. As can be seen from the figure, the C/C_O for AO7 degradation is higher in acidic medium compared to alkaline medium. This may be due to the increased electrostatic interaction between the positively charged surface of the catalyst and the negatively charged dye

molecules. The catalyst surface area becomes negatively charged as the pH increases to alkaline media and electrostatically repels the same charged dye molecules. In acidic pH media, the C/C_O for AO7 degradation is higher at pH 3, because the positive charges (H^+ ions) on the TiO_2 surface increase, and the negatively charged AO7s are easily adsorbed on the catalyst surface. Therefore, the degradation rate increases.

4.4 Effect of Catalyst Dosage

The effect of catalyst dosage on AO7 degradation is shown in **Fig. 9d**. The degradation rate was determined by adding the amount of catalyst (0.1 g, 0.15 g, 0.20 g, and 0.25 g) to 100 mL of a solution containing 10 mg/L dye at pH 3. The degradation rate increased linearly with the catalyst loading up to 0.1 g with further increasing catalyst loading, the degradation decreased. This may be due to the increased turbidity and agglomeration of the catalyst particles, which limits the penetration of light to activate the catalyst particle.[29] And collisions between active molecules and ground-state molecules of co-doped titania lead to deactivation of catalyst particles.[30] Therefore, the optimal catalyst dosage was found to be 0.1 g.

4.5 Effect of Initial Dye Concentration

In order to investigate the effect of initial dye concentration (AO7) on fixed catalyst weight (0.1 g) and pH 3, experiments were carried out using AO7 dyes at different concentrations from 10 mg/L to 40 mg/L, and the results are shown in **Fig. 9e**. The results show that the degradation rate of the AO7 dye has increased to 10 mg/L. However, further increasing the dye concentration leads to deactivation of the catalyst due to the capping effect. Therefore, the deterioration rate of AO7 was decreased.

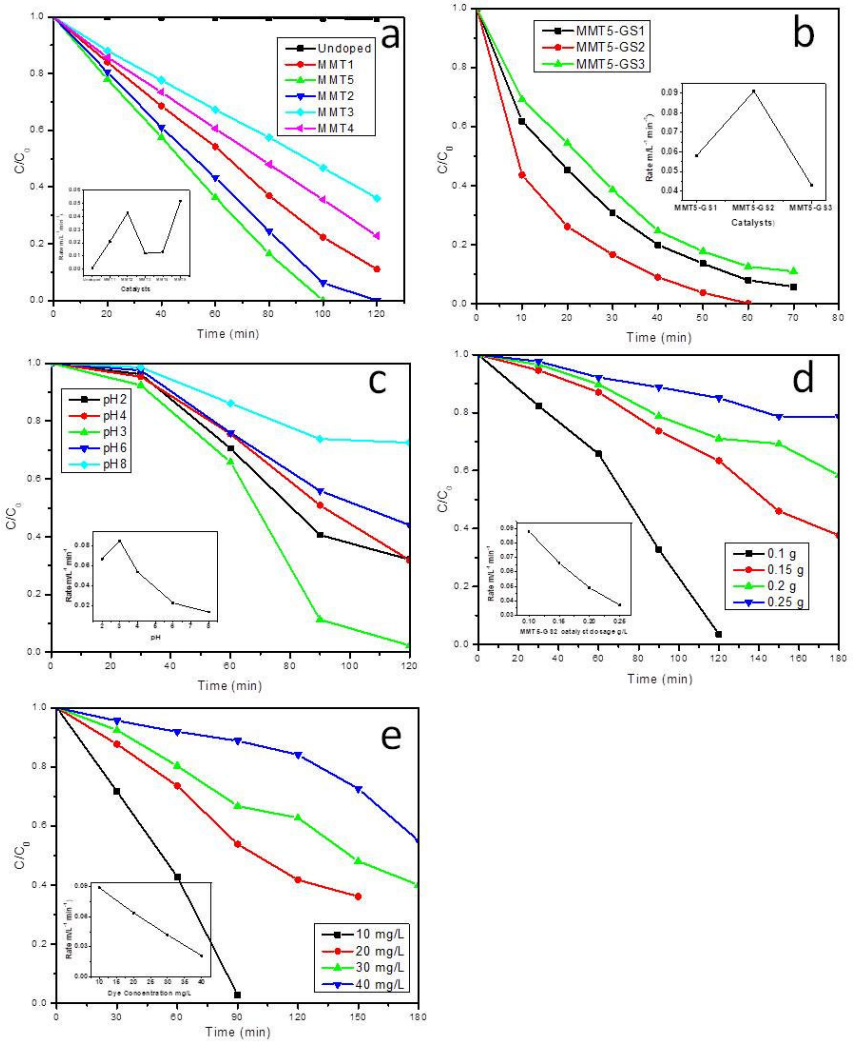

Fig. 9. (a) Effect of TiO_2 co-doped metal ion dopant concentration by the degradation of AO7 dye, **(b)** Effect of surfactant concentration on MMT5 on the degradation of AO7, **(c)** Effect of pH of the degradation of AO7 by MMT5-GS2 catalyst, **(d)** Effect of catalyst dosage on the degradation of AO7 by MMT5-GS2, **(e)** Effect of initial dye concentration on the rate of degradation of AO7 dye by MMT5-GS.

6. Conclusions

Surfactant assisted Manganese and Magnesium bimetal doped and undoped anatase TiO_2 NPs were prepared by sol-gel method and calcinated at 450 ^{0}C for 4 h. Among all the prepared nanomaterials MMT5-GS2 had comparatively narrow bandgap energy, high crystallinity of anatase phase, smaller crystallite size as well as high surface area. The photocatalytic activity of the MMT5-GS2 nanocatalyst has shown best results by degrading AO7 dye at optimized reaction conditions of pH at 3, catalyst dosage is 0.1 g and initial dye concentration 10 mg/L. It is found that OH radicals are the reactive species responsible for oxidative photocatalytic degradation of AO7. With the above results we conclude that MMT5-GS2 catalyst could be used as a promising material for abatement of water pollution caused by organic dyes.

References

1. Radetic M. **(2013)** Functionalization of textile materials with TiO_2 nanoparticles. *J. Photochem. Photobiol. C: Photochem. Rev.,*16 62-76.
2. Li S Q., Zhu R R., Zhu H., Xue M., Sun X Y., Yao S D., and Wang S L. **(2008)** Nanotoxicity of TiO_2 nanoparticles to erythrocyte in vitro. *Food. Chem. Toxicol.,* 46 (12) 3626-3631.
3. Wang Z., Chen C., Wu F., Zou B., Zhao M., Wang J., and Caihui F. **(2019)** Photodegradation of rhodamine B under visible light by bimetal codoped TiO_2 nanocrystals. *J. Hazard. Mater.,* 164 (2-3) 615-620.
4. Malika M., Rao Ch. V., Das R. K., Giri A. S., and Golder A. K. **(2016)** Evaluation of bimetal doped TiO_2 in dye fragmentation and its comparison to mono-metal doped and bare catalysts. *Appl. Surf. Sci.,* 368 316-324.
5. Chelli V. R., and Golder A. K. **(2017)** Bimetal doping on TiO_2 for photocatalytic water treatment: a green route. *Eur. Water.,* 58 53-60.
6. Wang Y., Zhang R., Li J., Li L., and Lin S. **(2014)** First-principles study on transition metal-doped anatase TiO_2. *Nanoscale Res. Lett.,* 9 46.
7. Lakshmi K. V. D., Rao T. S., Padmaja J. S., Raju I. M., Alim S. K. A., and Kalyani P. **(2018)** Visible light driven mesoporous Mn and S co-doped TiO_2 nano material: characterization and applications in photocatalytic degradation of indigo carmine dye and antibacterial activity. *Env. Nanotech. Monit. Manage.,* 10 494-504.
8. Zhang C., Chen S., Mo L., Huang Y., Tian H., Hu L., Huo Z., Dai S., Kong F., and Pan X. **(2011)** Charge recombination and band-edge shift in the dye-sensitized Mg^{2+} doped TiO_2 solar cells. *J. Phys. Chem. C.,* 115 (33) 16418-16424.
9. Meshesha D. S., Matangi R. C., Tirukkovalluri S. R., and Bojja S. **(2017)** Synthesis, characterization and visible light photocatalytic activity of Mg^{2+} and Zr^{4+} co-doped TiO_2 nanomaterial for degradation of methylene blue. *J. Asian Ceram. Soc.,* 5 (2) 136-143.
10. Sofianou M. V., Tassi M., Boukos N., Thanos S., Vaimakis T., Yu J., and Trapalis C. **(2014)** Solvothermal synthesis and photocatalytic performance of Mg^{2+} -doped anatase nanocrystals with exposed {001} facets. *Catal. Today.,* 230 125-130.
11. Chekuri R. D., and Tirukkovalluri S. R. **(2017)** Synthesis of Cobalt doped titania nano assisted by gemini surfactant: characterization and application of Acid Red under visible light irradiation. *South Afric. J. Chem. Eng.,* 24 183-195.
12. Akpan U. G., and Hameed B. H. **(2010)** The advancements in sol-gel method of doped -TiO_2 photocatalysts. *Appl. Catal. A: Gen.,* 375 (1) 1–11.
13. Ikhmayies S. J. **(2014)** Characetrization of nanomaterials. *JOM.,* 66 28-29.
14. Buitron G., Quezada M., and Moreno G. **(2004)** Aerobic degradation of the azo dye acid red 151 in a sequencing batch biofilter. *Bioresour. Technol.,* 92 (2) 143-149.
15. Lachheb H., Puzenat E., Houas A., Ksibi M., Elaloui E., Guillard C., and Herrmann J. M. **(2002)** Photocatalytic degradation of various types of dyes (Alizarin S, Crocein Orange G, Methyl Red, Methylene Blue). *Appl. Catal. B: Environ.,* 39 (1) 75-90.
16. Sahoo C., Gupta A. K., and Pal A. **(2005)** Photocatalytic degradation of Methyl Red dye in aqueous solution under UV irradiation using Ag^+ doped TiO_2. *Desalination* 181 (1-3) 91-100.
17. Wu J. C. S., and Chen C. H. **(2004)** A visible light-response Vanadium-doped titania nanocatalyst by solgel method. *J. Photochem. Photobiol. A: Chem.,* 163 (3) 509-515.
18. Lakshmi K. V. D., Rao T. S., Padmaja J. S., Raju I. M., and Kumar M. R. **(2019)** Structure, photocatalytic and antibacterial activity study of meso porous Ni and S co-doped TiO_2 nano material under visible light irradiation. *Chin. J. Chem. Eng.,* 27 1630-1641.
19. Raju I. M., Rao T. S., Lakshmi K. V. D., Chandra M. R., Padmaja J. S., and Divya G. **(2019)** Poly 3-Thenoic acid sensitized, Copper doped anatase/brookite TiO_2 nanohybrids for enhanced photocatalytic degradation of an organophosphorous pesticide. *J. Environ. Chem. Eng.,* 7 103211.
20. Shannon R. D. **(1976)** Revised effective ionic radii and systematic studies of interatomic distances in halides and chalogenides. *Acta. Cryst. A.*, 32 751-767.

21. Venkatachalam N., Palanichamy M., and Murugesan M. **(2007)** Sol-gel preparation and characterization of alkaline earth metal doped nano TiO_2: efficient photocatalytic degradation of 4-chlorophenol. *J. Mol. Catal. A: Chem.,* 273 (1-2) 177-185.
22. Jeong, E. D., Borse, P. H., Jang, J. S., Lee, J. S., Jung, O. S., Chang, H., Jin J. S., Won. M. S., and Kim H. G. **(2008)** Hydrothermal synthesis of Cr and Fe co-doped TiO_2 nanoparticle photocatalyst. *J. Ceram. Process. Res.*, 9 (3) 250-253.
23. Padmaja J. S., Rao T. S., Lakshmi K. V. D., and Raju I. M. **(2018)** Fabrication of hetero-structured mesoporous TiO_2-$SrTiO_3$ nanocomposite in presence of Gemini Surfactant: characterization and application in catalytic degradation of Acid Orange. *J. Environ. Chem. Eng.* 6 (5) 6457-6467.
24. Ghobadi N. **(2013)** Band gap determination of by using absorption spectrum fitting procedure. *Int. Nano Lett.,* 3 2.
25. Jaiswal R., Patel N., Kothari D. C., and Miotello A. **(2012)** Improved visible light photocatalytic activity of TiO_2 co-doped with Vanadium and Nitrogen. *Appl. Catal. B: Environ.,* 126 47-54.
26. Venkatachalam N., Palanichamy M., and Murugesan V. **(2007)** Sol–gel preparation and characterization of alkaline earth metal doped nano TiO_2: Efficient photocatalytic degradation of 4-chlorophenol. *J. Mol. Catal. A: Chem.,* 273 (1-2) 177-185.
27. Meshesha D. S., Matangi R. C., Tirukkovalluri S. R., and Bojja S. **(2017)** Synthesis, characterization and visible light photocatalytic activity of Mg^{2+} and Zr^{4+} co- doped TiO_2 nanomaterial for degradation of methylene blue. *J. Asian Ceram. Soc.,* 5 (2) 136-143.
28. Sharotri N., Sharma D., and Sud D. **(2019)** Experimental and theoretical investigations of Mn-N-co-doped TiO_2 photocatalyst for visible light induce degradation of organic pollutants. *J. Mater. Res. Tech.,* 8 (5) 3995-4009.
29. Miditana S. R., Tirukkovalluri S. R., Raju I. M., Alim S. A., Jaishree G., and Chippada M. L. V. P. **(2021)** Gemini surfactant assisted Mn/Mg bimetal doped TiO_2 nanomaterials: characterization and photocatalytic activity studies under visible light irradiation. *Sustain. Environ. Res.,* 31 (6) 1-12.
30. Deng Q. R., Gao Y., Xia X. H., Chen R. S., Wan L., and Shoa G. **(2009)** V and Ga co-doping effect on optical absorption properties of TiO_2 thin films. *J. Phys.: Conf. Ser.,* 152 12073.